Feasibility of Long-Term Monitoring of Multifrequency and Multisegment Body Impedance by Portable Devices

Federica Villa, Alessandro Magnani, Giampiero Merati, and Paolo Castiglioni*

I. Introduction

BIOELECTRICAL impedance spectroscopy (BIS) provides a fast, noninvasive, cheap, and reliable way to assess the composition of individual segments of the body [1]. The method is based on the measure of the voltage drop across body segments crossed by an injected current, and in the calculation of magnitude and phase of the corresponding electrical impedance over a broad range of frequencies. So far, BIS has been applied to study a variety of physiological and clinical conditions. In particular, it may help to quantify the level of hydration [2] or the ratio between fat and lean masses [3]; to diagnose muscle disorders, monitoring the muscle health during rehabilitation programs [4], [5]; and to detect in advance pulmonary edema [6] or lymphedema in legs and arms [7].

BIS studies, however, have been limited to laboratory or clinical settings. In fact, available instrumentation consists in bulky systems which cannot be used in freely moving subjects for long periods of time. This limit could be overcome by a proper miniaturization of the devices. Actually, small portable systems able to measure the body impedance unobtrusively for several hours would open the use of BIS to many new applications. For instance, they would make it possible monitoring the hydration level over the 24 h in subjects with an altered control of thirst, as in elderly people, or in workers and endurance athletes undergoing extreme physical activities; they would allow to quantify changes in the distribution of body fluids following gravitational stresses in fighter pilots or astronauts; in studies of occupational medicine, they could be employed for assessing impedance variations in specific muscular districts during the everyday working activities.

The fulfilment of such devices requires the design of circuits with an optimized number of components to minimize weight, size, and power consumption. In this regard, the use of a digital signal processor (DSP) appears the best solution for generating stimulation currents and for elaborating the sensed signals. Therefore, the aim of this study is to evaluate the feasibility of a DSP-based approach in order to design portable devices for segmental BIS without significantly interfering with the subjects activities. For this aim, we present a prototype that implements the main features required for a portable BIS system. In particular, our prototype employs a small DSP board with very-low power consumption, which provides magnitude and phase of body impedance over a broad range of frequencies. This goal is achieved by employing square-wave stimulating waveforms that, compared to sinusoids, are easier to be generated with digital components and do not require high speed digital to analog converters. At the best of our knowledge, this is the first use of square-wave stimulations in BIS (a preliminary version of the device was presented at the *PRIME 2012 Conference* in Aachen, Germany [8]).

In this study, we also present the results of experimental tests performed with our prototype on a group of male and female volunteers. BIS of different body segments was assessed according to an experimental protocol, which included postural changes. These experimental data allow us to evaluate the capability of

Manuscript received December 13, 2013; revised February 25, 2014; accepted February 25, 2014. Date of publication March 5, 2014; date of current version May 15, 2014. *Asterisk indicates corresponding author.*

F. Villa and A. Magnani are with the Dipartimento di Elettronica, Informazione e Bioingegneria, at Politecnico di Milano, 20133 Milano, Italy (e-mail: federica.villa86@gmail.com; alessandro.magnani86@gmail.com).

G. Merati is with the Department of Biomedical Sciences for Health, Università degli Studi di Milano, 20122 Milano, Italy (e-mail: giampiero.merati@unimi.it).

*P. Castiglioni is with the IRCCS Fondazione Don C. Gnocchi, I-20148 Milano, Italy (e-mail: pcastiglioni@dongnocchi.it).

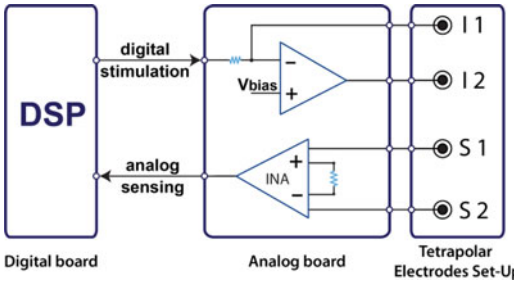

Fig. 1. Schematic representation of the overall system composed by a digital processing board, an analog board and a tetrapolar setup.

our BIS system 1) to follow impedance changes due to the redistribution of fluids after postural changes, and 2) to detect gender differences likely associated to the diverse composition and size of body segments in males and females.

II. System Implementation

Our prototype is composed by a digital board and an analog board connected to a tetrapolar electrodes setup (see Fig. 1). The tetrapolar setup consists in a couple of stimulation electrodes (I1 and I2) and in a couple of sensing electrodes (S1 and S2). The analog board includes a transconductance amplifier that injects the stimulation current, and an instrumentation amplifier (INA) that senses the voltage drop across the body. The analog board receives a stimulation voltage from the digital board, to which it sends back the measured voltage drop. The digital board includes a DSP. The DSP generates the stimulation waveforms, processes the measured data, and includes an ADC to digitize the sensed voltage. Details of the system follow.

A. Tetrapolar Electrodes Setup

If the same two electrodes are used for stimulation and sensing, electrodes with a large area (band electrodes) are required to reduce the current constrictional effects, which characterizes small disk electrodes. In addition, sensing electrodes may influence the measure with their own impedance if crossed by the injected current and we showed that the contribution of small disk electrodes to whole body impedance at 10 kHz is not negligible if bipolar or tripolar electrode setup are employed [8]. By contrast, a tetrapolar setup provides impedance measures less dependent on the skin–electrode interface [4], [8], allowing the use of small disk electrodes, as the pregelled electrodes of most ECG Holter recordings. Small disk electrodes are particularly suitable for portable multisegment BIS systems, because they are easier to place and interfere less with the subject movements. Moreover, pregelled ECG electrodes appear able to provide stable impedance measures over several hours [8].

Therefore, in our prototype a tetrapolar setup with ECG disk electrodes is used. A periodic current, with zero mean, is injected into the body through the I1 and I2 electrodes. The voltage drop generated by the injected current is measured by the S1 and S2 sensing electrodes. The position of the four electrodes depends on the specific segment of the body to be measured. Typical locations of I1 and I2 are the ipsilateral foot and hand. The most common positions of S1 and S2 are showed in Table I, together with the corresponding body segment of which the impedance is measured. The anatomic positions of S1 and S2 refer to the same side of the body. More complex dispositions can be also employed. For instance, the system will measure the impedance of the right leg with I1 and I2 on the right foot and hand and S1 and S2 on the right and left ankles [3].

TABLE I
Typical Positions of Injecting and Sensing Electrodes for each Body Segment

I1	I2	S1	S2	Body Segment
foot	hand	ankle	wrist	whole body
foot	hand	shoulder	wrist	arm
foot	hand	hip	shoulder	trunk
foot	hand	ankle	hip	leg

Sensing and injecting electrodes on the same side of the body.

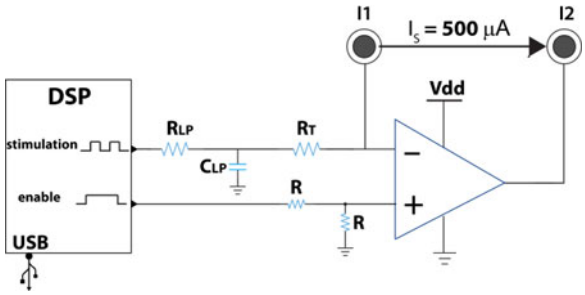

Fig. 2. Transconductance amplifier driven by the DSP. The square wave stimulation voltage reaches the amplifier after a low-pass filtering by C_{LP} and R_{LP}; the current is injected only during the measurement ("enable" signal ON). $R_{LP} = R_T = 1.65$ kΩ; $C_{LP} = 100$ pF; $R = 10$ kΩ; Vdd $= +3.3$ V.

The amplitude ratio between the harmonics at frequency f of the S1–S2 dropout and of the injected current provides the impedance magnitude, whereas the difference between their phases provides the impedance phase at f.

B. Analog Board

The analog board is designed to minimize the number of components, and consequently, its overall dimension and power consumption. It is powered with a single supply at $+3.3$ V generated with an on-board dc–dc converter either from the $+5$ V of the USB connection on the DSP board or from an external battery. The same quad-operational amplifier (MCP654) has been used for the transconductance amplifier and for the INA.

The transconductance amplifier (see Fig. 2) receives the stimulating voltage waveform from the DSP and generates a proportional current. Once the measure is completed the transimpedance amplifier is disabled by a dedicated DSP output, interrupting the current flow in the body. The resistance R_{LP} and capacitance C_{LP} actuate an antialiasing prefiltering at 1 MHz.

The INA requires a relative high bandwidth (about 1 MHz), and a single low-voltage power supply to fulfill the low power consumption specification of the overall system. Since commercial INAs do not satisfy both these constrains, the INA has been custom designed using three operational amplifiers with

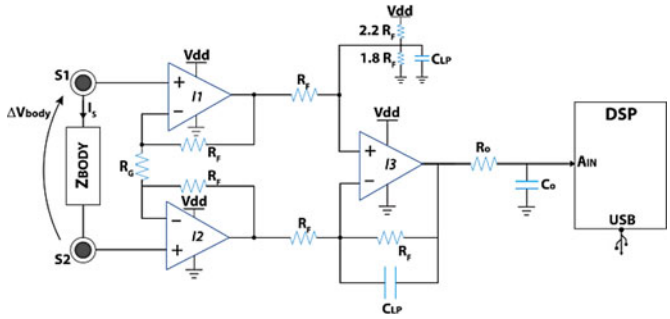

Fig. 3. Scheme of INA, with second-order antialiasing filtering. $R_F = 10\,\text{k}\Omega$; $R_G = 20\,\text{k}\Omega$; $C_{LP} = 16$ pF; $R_O = 10\,\text{k}\Omega$; $C_O = 16$ pF.

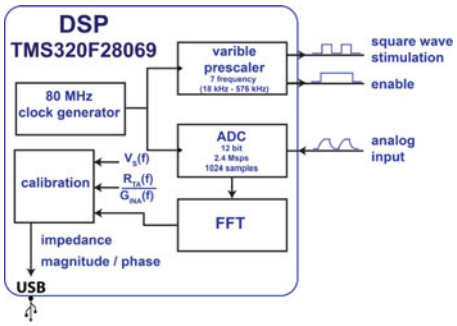

Fig. 4. Schematic representation of the digital board and its functionalities. Main component is a Texas Instruments DSP with internal 12-bit ADC.

5 MHz gain-bandwidth product (see Fig. 3). Considering a maximal body impedance of 1.5 kΩ and a stimulation current of ±500 μA, the differential voltage at the input of the INA falls within the ±0.75 V range. The INA theoretical gain at 0 Hz is $(1+2{\cdot}R_F/R_G)$. Setting this gain to 2, the full scale range of the ADC (0.3 V) is covered without saturating any internal node.

An offset to the output voltage acting on noninverting terminal of the third OpAmp (I3 in Fig. 3) matches the input differential swing (positive and negative) with the output single-ended swing (only positive). The C_{LP} and C_o capacitances introduce a second-order antialiasing low-pass filter at 1 MHz.

C. Digital Board

The digital board is the core of the system (Fig. 4). It generates the stimulation waveforms, converts digitally the sensed voltage, computes the fast Fourier transform (FFT) of the signals, calculates magnitude and phase of the body impedance and performs the calibration procedure.

The DSP is a Texas Instrument C2000 "*Piccolo family,*" with 80 MHz clock, internal 12-bit ADC (up to 3 Msps) and an USB interface. Selection criteria for the choice of the DSP were high operation speed, good performances of the ADC, and above all, the compactness of the evaluation board. Stimulus generation and data acquisition are implemented as two parallel and synchronous processes generated by the same clock not to introduce phase errors.

The stimulation waveform is a square wave, much easier to generate with the DSP than a pure sinusoid. The square wave drives an alternate current (±500 μA) with 50% duty cycle and zero mean, to avoid injecting a dc component. In order to cover the frequency range of interest with a low number of stimulation waveforms, seven square waves are generated. Six square waves have their first harmonic equispaced on a log-frequency scale and the considered frequencies are: 18, 36, 72, 144, 288, and 576 kHz. The seventh waveform has its first harmonic at 50 kHz, because this frequency is employed in most monofrequency body impedance systems. The duration of each train of square waves is 5 ms, given by the sum of the ADC acquisition time (0.5 ms) and the FFT process time (4.5 ms). Since seven waveforms are generated, the overall measure time is 35 ms.

The sampling frequency has been fixed at 2.3 MHz, multiple of each stimulation frequency to avoid bin leakage. In this way, only one bin of the FFT is excited. The 12-bit ADC acquires 1024 samples for each stimulation frequency in real time. The DSP computes the 1024-points FFT and provides magnitude and phase of the first harmonic of the INA's output voltage. Magnitude and phase of the body impedance at the frequency f are

$$|Z_{\text{body}}(f)| = \frac{|V_{\text{body}}(f)|}{|I_s(f)|} \tag{1}$$

$$\angle Z_{\text{body}}(f) = \angle|V_{\text{body}}(f)| - \angle|I_s(f)| \tag{2}$$

with V_{body} the Fourier transform of the voltage drop between sensing electrodes and I_s the Fourier transform of the stimulation current. However, neither V_{body} nor I_s are directly measured. The output of the INA, V_{INA}, differs from V_{body} because

$$V_{\text{INA}}(f) = V_{\text{body}}(f) \cdot G_{\text{INA}}(f) \tag{3}$$

with G_{INA} the gain of INA. This gain includes the dc gain and accounts for singularities, components tolerances and parasitisms of the INA. Moreover, the relation between stimulation voltage, V_s, and I_s is

$$V_s(f) = R_{\text{TA}}(f) \cdot I_S(f) \tag{4}$$

with $R_{\text{TA}}(f)$, the transfer function of the transconductance amplifier, which accounts for its singularities, parasitisms, and components tolerances. This gives the relation

$$\frac{V_{\text{body}}(f)}{I_s(f)} = \frac{R_{\text{TA}}(f)}{G_{\text{INA}}(f)} \times \frac{V_{\text{INA}}(f)}{V_s(f)} \tag{5}$$

where only $V_{\text{INA}}(f)$ and $V_s(f)$ are known quantities. To identify $R_{\text{TA}}(f)/G_{\text{INA}}(f)$, the system is calibrated by connecting a known resistance to the four electrodes, and by measuring $V_{\text{INA}}(f)$ at each stimulation frequency of $V_s(f)$. In this way, once the $R_{\text{TA}}(f)/G_{\text{INA}}(f)$ complex ratio is known, we obtain the impedance magnitude and phase as

$$|Z_{\text{body}}(f)| = \left|\frac{R_{\text{TA}}(f)}{G_{\text{INA}}(f)}\right| \times \frac{|V_{\text{INA}}(f)|}{|V_s(f)|} \tag{6}$$

$$\angle Z_{\text{body}}(f) = \angle\frac{R_{\text{TA}}(f)}{G_{\text{INA}}(f)} + \angle|V_{\text{INA}}(f)| - \angle|V_s(f)|. \tag{7}$$

The computation of $R_{\text{TA}}(f)/G_{\text{INA}}(f)$ is performed by the DSP at the end of the calibration procedure.

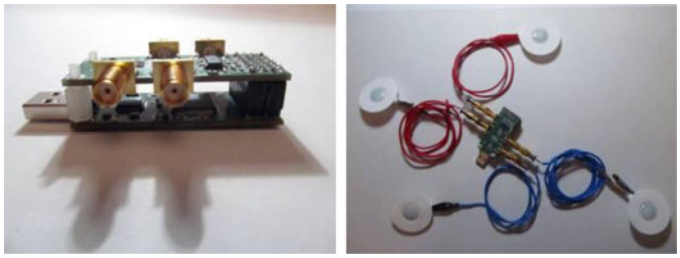

Fig. 5. Left: the prototype with the lower digital board connected to a USB for data downloading, and the upper analog board for interfacing injecting and sensing electrodes. Right: the prototype connected to the electrodes.

TABLE II
ANTHROPOMETRIC CHARACTERISTICS OF VOLUNTEERS AS MEAN (STANDARD DEVIATION) OVER THE GROUPS

	Males (N=10)	Females (N=10)
Body		
weight [kg]	74.5 (10.1)	57.5 (9.5) **
height [cm]	179.5 (6.1)	166.6 (6.2) **
Arm		
L [cm]	63.7 (5.2)	57.3 (10.1)
C [cm]	26.0 (2.0)	23.2 (3) *
L/A [cm]$^{-1}$	1.2 (0.2)	1.4 (0.4)
Trunk		
L [cm]	53.4 (3.6)	46.6 (3.5) **
C [cm]	91.9 (9.7)	74.6 (6) **
L/A [cm]$^{-1}$	0.08 (0.02)	0.11 (0.02) **
Leg		
L [cm]	95.9 (8.7)	88.3 (5.3) *
C [cm]	39.4 (7.2)	36.4 (4.3)
L/A [cm]$^{-1}$	0.8 (0.2)	0.9 (0.2)

L and *C* are length and circumference of the body segment, $A=C^2/(4\pi)$ is the cross-sectional area. The * and ** indicate differences between males and females significant at $p<0.05$ and <0.01 (unpaired *t*-test).

D. Complete System

The complete system is shown in Fig. 5. The size of the electronic boards is 5.5 cm $\times$ 2.4 cm $\times$ 2 cm, the weight is less than 50 g (battery and electrodes excluded). The total power consumption is lower than 100 mW during each measurement. A sequences of measures can be performed consecutively and averaged to increase the precision. We choose to perform 50 consecutive measures for each frequency. In this way, a set of measurements (seven frequencies) is computed in less than 2 s.

III. VALIDATION WITH EXPERIMENTAL DATA

We tested the performances of our prototype in a group of volunteers. Aim was to evaluate whether our system 1) tracks the variations of impedance which follow changes of posture, and 2) identifies gender differences in impedance possibly due to differences between males and females in size, geometry, and composition of specific body segments.

Subjects and Data Collection: We enrolled 20 healthy volunteers (ten males and ten females) ageing between 20 and 25 years. Average anthropometric characteristics are summarized in Table II. Six disposable pregelled ECG electrodes were placed on each subject. Two electrodes were placed on the dorsal surface of the left hand and foot as I2 and I1 injecting electrodes. Four electrodes were placed on the left malleolus (S_A), upper anterior iliac spine (S_B), shoulder (S_C), and wrist (S_D) and connected in succession to the electronic board as the S1 and S2 sensing electrodes. First, the S_A and S_D electrodes were employed as sensing electrodes to measure the "whole body" impedance. Then, the S_A–S_B, S_B–S_C, and S_C–S_D couples were used in succession as sensing electrodes to measure the impedance of "leg," "trunk" and "arm." During the experiment, the arm was supported with a scarf in the dependent position.

Experimental Protocol: Each subject was asked to rest in supine position for 20 min. Baseline impedance measures (BAS) of "arm," "trunk," "leg," and "whole body" segments were taken at the end of this period. Then, the subject was asked to stand up and maintain the standing position for 10 min. BIS measures were taken immediately after the change of posture (early standing, EST) and at the end of standing (late standing, LST). The subject was finally asked to lie supine for an additional period of 10 min and measures were repeated immediately after the change of posture from standing to supine (early supine, ESU) and at the end of the period (late supine, LSU).

Normality test: Before statistical analysis, the normality of the distributions were tested at each frequency (Shapiro Wilks test). The hypothesis of normality was rejected for the impedance phases only. Therefore, the impedance magnitudes were plotted as group mean $\pm$ standard error of the mean and compared by parametric statistical tests, the impedance phases were plotted as median with first–third quartiles and compared by nonparametric statistics.

A. Posture and Impedance

Impedance differences between standing and supine were assessed by comparing LST with LSU. The modulus of "whole body" impedance was lower in standing, with significant differences at all the frequencies (see Fig. 6, upper panel). The impedance phase was slightly lower in supine position at frequencies $\leq$36 kHz (see Fig. 6, lower panel). Posture affected differently each body segment (see Fig. 7). During standing the impedance magnitude of the leg was lower at all the frequencies, while the impedance phase was higher at $f<100$ kHz. By contrast, no differences were found in $|Z(f)|$ of the arm and trunk.

B. Gender and Impedance

The main gender differences in impedance (see Fig. 8) regard the trunk, that in males has a lower magnitude at all the frequencies. Also, the impedance magnitude of the arm is significantly lower in males at all the frequencies. Impedance phases of arm and leg tend to be higher in males, while the phases of the trunk are higher in females.

C. Body Fluids Dynamics and Posture Changes

Individual body segments are often modeled as cylinders of different tissues arranged in parallel [1]. The electric resistance R of each cylinder is

$$R = \rho \frac{L}{A} \tag{8}$$

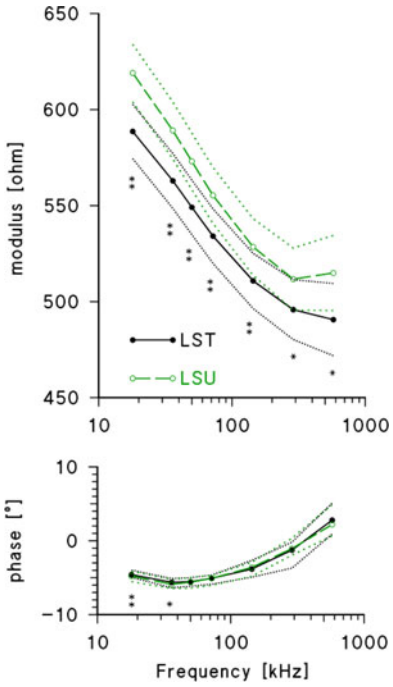

Fig. 6. "Whole body" impedance magnitude (upper panel, mean ±standard error) and phase (lower panel, median and first–third quartiles) in 20 volunteers during late standing (LST) and late supine (LSU) conditions. The "$*$" and "$**$" indicate differences statistically significant with $p<0.05$ and $p<0.01$ (paired t-test for the modulus, Wilcoxon test for the phase).

with L length, A cross-sectional area, and ρ resistivity of the cylinder. The resistivity at 1 kHz is similar to that of plasma because at this frequency the conductivity is much higher for plasma than for muscle tissues, bones, or fat [9], [10]. Therefore, the impedance magnitude at 1 kHz, R_E, is representative of the extracellular water volume in the body segment, with R_E increasing when the extracellular volume decreases.

In our study, impedance magnitudes of each body segment are linearly related to the logarithm of the frequency f when $f < 100$ kHz. This is true both in supine and standing position (see Fig. 7) and in males and females separately (see Fig. 8). R_E was, therefore, estimated as the intercept of the linear regression between $|Z(f)|$ and log (f) for $f <100$ kHz (in a log f scale with f in kHz, the intercept corresponds to the value at $f = 1$ kHz). R_E was calculated in baseline, in early and late standing, in early and late supine position. Differences between genders and among the five experimental conditions were assessed separately in the arm, trunk, and leg by a two-factor (posture and gender) analysis of variance (ANOVA). When the factor "Posture" or the interaction between factors were statistically significant at $\alpha = 0.05$, baseline was compared with the other conditions by Fisher least significant difference *post hoc* procedure.

Fig. 9 shows R_E values and Table III reports factors significances. Gender was a statistically significant factor for the arm and the trunk, and Fig. 9 shows R_E profiles clearly higher in females both in the arm and in the trunk. Gender was not significant for the leg, and Fig. 9 shows overlapping R_E profiles in the leg. Posture was a significant factor for the arm and the leg, not for the trunk, and Fig. 9 also shows clear modulations of R_E through the five steps of the experiment for arm and leg, with similar profiles in males and females. In particular, *post hoc* analysis indicated a significant reduction of impedance at early and late standing compared to baseline and that the recovery was completed in late supine for the leg segment only.

As to the trunk, the interaction between factors reached the statistical significance (see Table III), indicating that the effects of the change of posture were different in males and females. Actually, Fig. 9 suggests opposite trends for males and females; in particular, R_E increased significantly from baseline to late standing only in males.

IV. Discussion

Experimental data indicate that our system provides impedance measures over a wide range of physiological values, from several hundred of ohms (whole body impedance) to few tens of ohms (trunk impedance). Results are coherent with measures reported in literature and may contribute to better understand some critical issues in BIS. In this regard, the following points should be considered.

BIS between genders and body segments: We measured a much lower impedance in the trunk than in the limbs, indicating that the trunk contributes only modestly to the whole body impedance. In a previous study, monofrequency impedance measures at 50 kHz were obtained in a large population of healthy subjects in supine posture [3]. This previous study reported values for the impedance modulus in the arm, trunk, and leg equal to 194, 37.5, and 229 Ω in men, and to 281, 51.2, and 268 Ω in women. These values and their differences among body segments and between genders testify for the overall quality of our measures because they are similar to the $|Z(f)|$ values at $f = 50$ kHz we showed in Fig. 8.

Differences among body segments and between genders can be in part explained by (8), if we assume the simplified model that represents each body segment as cylinder of resistivity ρ. In this case, the L/A ratios of Table II (lower in the trunk than in the limbs and higher in women than in men) provide a possible explanation, because they imply a lower electric resistance in the trunk than in the limbs, and in males than in females.

Extracellular volume and body posture: We found significant R_E variations in the arm and leg following changes of posture (see Fig. 9). These variations match the variations of extracellular volume reported in a previous study where segmental BIS was measured in six male volunteers who changed from a standing to a supine position [11]. Therefore, our system appears able to track the change of the distribution of body fluids following changes of posture. Moreover, it allowed us to statistically demonstrate a faster dynamics for the leg than for the arm after postural changes, a result which was only anecdotally suggested in [11].

Furthermore, the same previous study (that only considered male individuals) reported a small but significant decrease of extracellular volume in the trunk segment changing posture from standing to supine [11]. We observed the same significant change in R_E but only in the male group, indicating that gender differences should characterize not only the absolute impedance

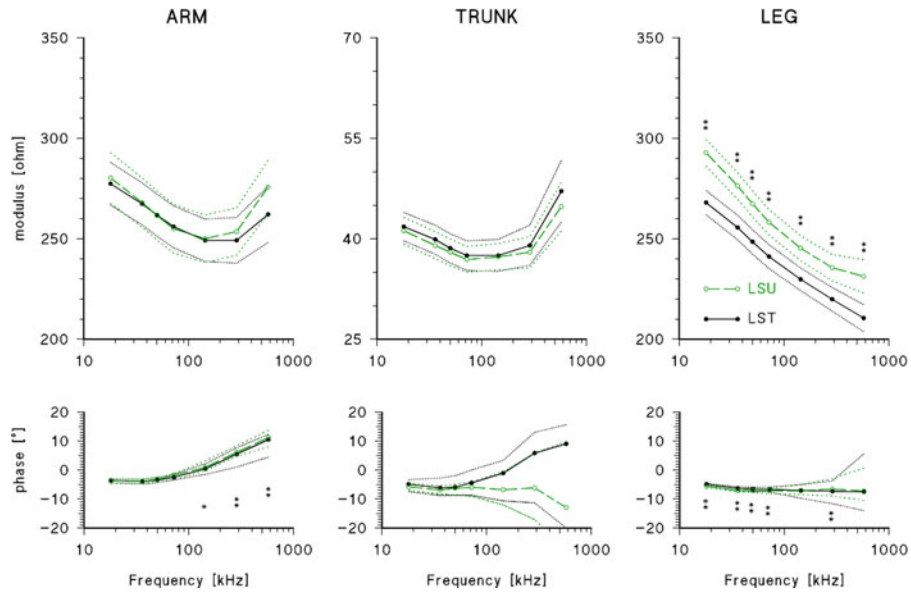

Fig. 7. Comparison between late supine (LSU) and late standing (LST) conditions of impedance magnitude (*upper panels*, mean ± standard error) and phase (*lower panels,* median and first-third quartiles) in three body segments for the whole group ($N = 20$) of volunteers. The symbols "$*$" and "$**$" indicate differences between postures significant at the $p<0.05$ and $p<0.01$ statistical levels (paired t-test for the magnitude, Wilcoxon test for the phase).

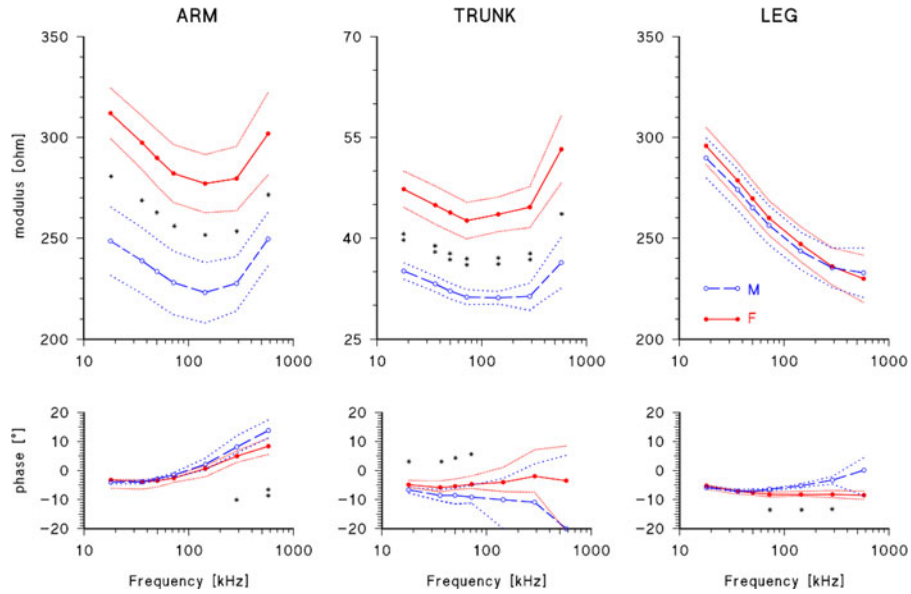

Fig. 8. Comparison between males (M, N = 10) and females (F, N = 10) of impedance magnitude (*upper panels*, mean ± standard error) and phase (*lower panels,* median and first-third quartiles) in three body segments: measures obtained in LSU condition. The symbols "$*$" and "$**$" indicate gender differences significant at the $p < 0.05$ and $p < 0.01$ statistical levels (unpaired t-test for the magnitude, Mann Whitney U test for the phase).

values of the trunk, but also the dynamics of impedance changes after a change of posture.

Positive impedance phases: The electric properties of biological tissues can be modeled by the electric resistance of extracellular fluids in parallel to *RC* elements, the latter describing the resistance of the intracellular fluids and the capacitance of cell membranes [4]. Accordingly, positive phases should not appear in *Z(f)* of body tissues. This is approximately true in the "whole body" and leg impedance (see Fig. 6 and 7), while positive phases appear clearly in the arm segment at $f>100$ kHz (see Fig. 7).

Discrepancies at the higher frequencies from the resistive–capacitive model have been repeatedly reported in the past [12], [13]. It has been suggested that they may arise from the time delay due to the conductor length, which produces significant phase errors at the higher frequencies [14]. However, since the same hardware was used in the same experimental setup and positive phases appeared in the arm but not in the leg (two body segments with similar electric resistance), it is unlikely that the conductor delay may explain the positive phase appearing in the arm but not in the leg.

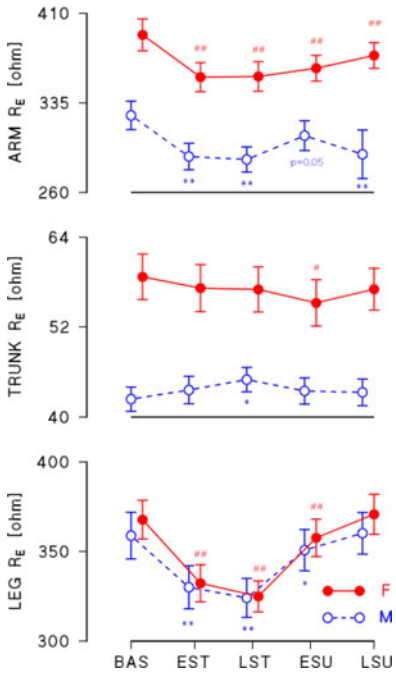

Fig. 9. R_E as mean $\pm$standard error in males (open circles) and females (solid circles) under the five experimental conditions. The symbols $*$ and $**$ in males and # and ## in females indicate differences with BAS significant at $p < 0.05$ and $p < 0.01$.

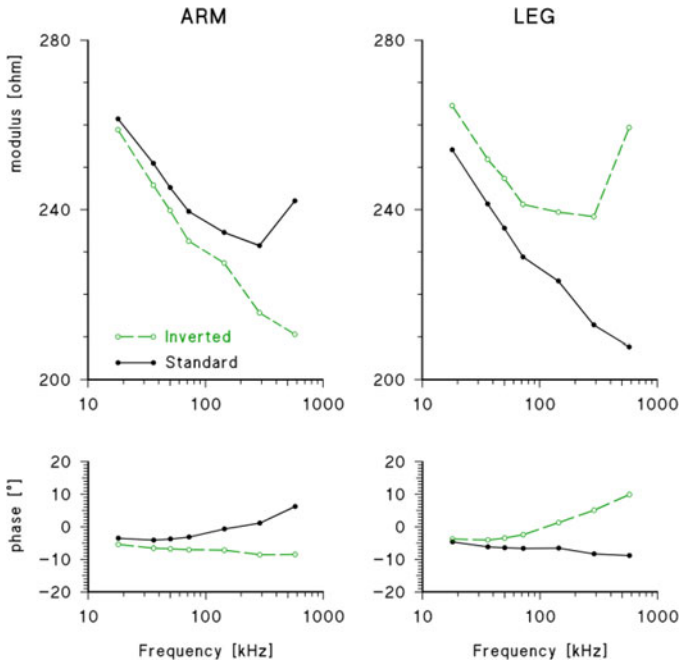

Fig. 10. Impedance modulus and phase of arm and leg segments in one standing subject with standard disposition of injecting electrodes (see Table I, closed circles) and after having inverted the injecting electrodes (I1 on hand, I2 on foot, open circles).

TABLE III
INFLUENCE OF SEX AND BODY POSTURE ON R_E: SIGNIFICANCE p OF THE FACTORS GENDER, POSTURE AND OF THEIR INTERACTIONS AFTER ANOVA

	Gender	Posture	Interaction
Arm	**<0.01**	**$<10^{-6}$**	0.31
Trunk	**<0.001**	0.33	**<0.05**
Leg	0.71	**$<10^{-9}$**	0.13

Possible causes for positive impedance phases in biomaterials were investigated by Grimnes and Martinsen [15] who suggest two contributions that may play a role in our case. One is the presence of different current paths in parallel. The existence of more than one current path cannot be excluded because body segments are composed by inhomogeneous tissues with different current densities. A second possible source of positive phases is the self-inductance of the tissue. Self-inductance is expected to provide a significant addition at the highest frequencies when the impedance modulus is relatively low [15], as in the trunk. Therefore, it is possible that also phenomena of tissue self-inductance may have contributed to increase the impedance phase at frequencies higher than 100 kHz, but it remains unclear why different current paths or self-inductance should produce more inductive effects in the arm than in the leg.

A known source of artifacts in body impedance has been identified in stray capacitances between body segments and earth and between the device signal and ground [12], [16]. In particular, it has been recently shown that stray capacitances between body and earth may generate a resonance above 10 MHz, which looks like an inductive effect at lower frequencies [17]. It might appear unlikely that stray capacitance are responsible for the positive phases that we observed in the arm and not in the leg, because the calibration should have cleared their artifactual contributions and because the same hardware was used for all the body segments. However, it should be considered the distributed nature of body stray capacitances and that in multisegment BIS the relative position of sensing electrodes with respect to injecting electrodes (and therefore, to the virtual ground of the device) depends on the selected segment. In the appendix, we show theoretically and with a circuit simulation that, among the stray capacitances distributed between the injecting electrodes, the major role in generating inductive effects is played by those located upstream the sensing electrodes (between I1 and S2). Thus, this analysis may explain why we observed inductive effects in the arm and not in the leg. If the theoretical analysis reported in appendix describes correctly the phenomenon, we should observe inductive effects in the leg and not in the arm just by exchanging the injecting electrodes. We verified this conjecture by measuring arm and leg impedance in an additional volunteer first by employing the standard electrodes configuration, then by exchanging the injecting electrodes (I1 on the hand and I2 on the foot). Results (see Fig. 10) show that when the injecting electrodes are inverted, the inductive effects disappear in the arm and appear in the leg segments, thus, supporting experimentally the theoretical analysis in appendix.

V. CONCLUSION

We showed that it is possible to design small portable systems based on low-power DSPs for measuring BIS of different body segments. This class of devices may allow monitoring the electric impedance for long periods, interfering minimally with

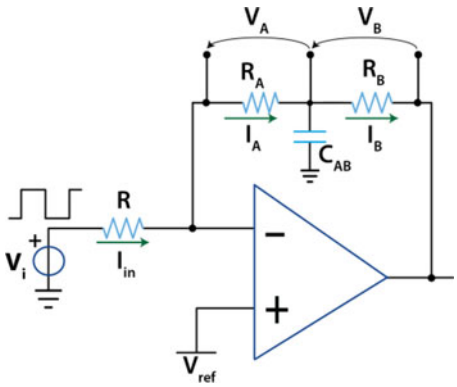

Fig. 11. Simplified schematic of BIS setup, with impedances of two body segments modeled by the R_A and R_B resistances and stray capacitances modeled by C_{AB}.

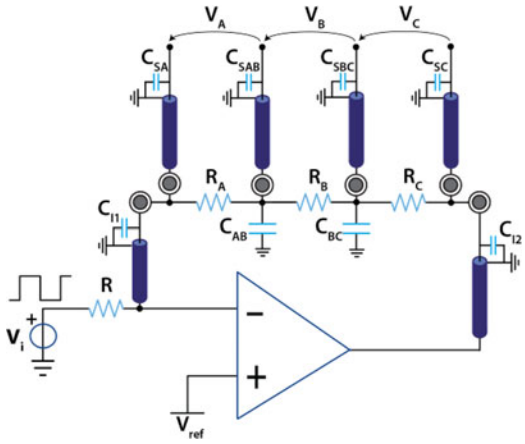

Fig. 12. Schematic of BIS setup for three body segments (A, B and C) with stray capacitances between body and ground (C_{AB} and C_{BC}) and between ground and coaxial sensing (C_{SA}, C_{SAB} and C_{SB}) or injecting (C_{I1} and C_{I2}) cables.

the subjects' activities. In particular, the prototype we presented permits to perform measures over the broad range of frequencies required in even sophisticated BIS studies. A complete multisegment, portable BIS system can be easily realized from our prototype by including an automatic switch among couples of sensing electrodes and by including local data storage, with only a small increase in weight and power consumption.

Our results pointed out a contribution of stray capacitances that produce inductive effects above 100 kHz. However, theoretical analysis and experimental data also suggested that switching the two injecting electrodes may effectively remove this artifactual contribution, at least from the external (limbs) segments.

The future availability of such portable and unobtrusive BIS systems may open the way to different new applications of electrical impedance in sports and occupational medicine, in health monitoring of the elderly and patients, and in rehabilitation medicine.

Appendix
Inductive Components in Segmental BIS from Stray Capacitances

BIS setups may show inductive effects in contrast with the traditional model of body impedance consisting in resistive and capacitive components only. Some authors suggested that stray capacitances between body and ground or between the device components and ground may be responsible for inductive effects [16], [17]. Oddly, in our study, we observed inductive effects (i.e., an increase of Z magnitude and positive Z phases at $f > 100$ kHz) in the arm and trunk segments but not in the leg segments, even if we used the same hardware in the same experimental condition to monitor each body segment. This appendix demonstrates with a theoretical analysis and a circuit simulation that the phenomenon can be explained considering the different effects produced by stray capacitances located upstream or downstream the body segment to be measured.

The circuit of Fig. 11 illustrates theoretically that inductive effects are produced only by stray capacitances located downstream the body segment. For simplicity, only two body segments are considered, A and B, with their impedance modeled by the resistances R_A and R_B. The Fourier transform of the measured voltages are V_A and V_B, respectively, and the Fourier transform of the injected current is I_{in}. The impedance of the segment A is $Z_A = V_A \,/\, I_{\text{in}}$. Since $V_A = I_A \cdot R_A$, then

$$Z_A = \frac{I_A \cdot R_A}{I_{\text{in}}} = R_A \tag{A1}$$

because $I_A = I_{\text{in}}$ upstream the stray capacitance. Thus, inductive effects do not appear upstream the stray capacitance. Downstream the stray capacitance, I_B differs from I_{in} because the current I_{AB} flows through C_{AB}

$$I_{AB} = \frac{V_A}{1/sC_{AB}} = sC_{AB}R_A I_A. \tag{A2}$$

Since $I_B = I_A + I_{AB}$, then

$$I_B = I_{\text{in}}(1 + sR_A C_{AB}) \tag{A3}$$

and finally

$$Z_B = \frac{V_B}{I_{\text{in}}} = R_B(1 + sR_A C_{AB}). \tag{A4}$$

Equation (A4) shows that the stray capacitance adds an inductive component to R_B.

A more realistic model is shown in Fig. 12. The body consists in three segments, representing the arm (segment C), the trunk (segment B), and the leg (segment A), with resistances $R_A = R_C = 250\ \Omega$, and $R_B = 50\ \Omega$. Stray capacitances between body and ground and between device components and ground are modeled separately. The capacitance between body and ground depends on the position of the subject and may range from 10 to 100 pF [18]. In this analysis, we set $C_{AB} = C_{BC} =$ 10 pF. Coaxial cables, necessary to reduce the effect of external disturbances, give an important contribution to stray capacitances to ground, ranging between 100 and 500 pF/m. In our model, we set the stray capacitances C_{SA}, C_{SAB}, C_{SBC}, and C_{SC} of sensing cables and the stray capacitance C_{I1} and C_{I2} of injecting cables equal to 300 pF. It should be noted that C_{I1} and C_{SA} do not influence the measures because fixed at virtual ground and their current flows are zero; and that even if currents

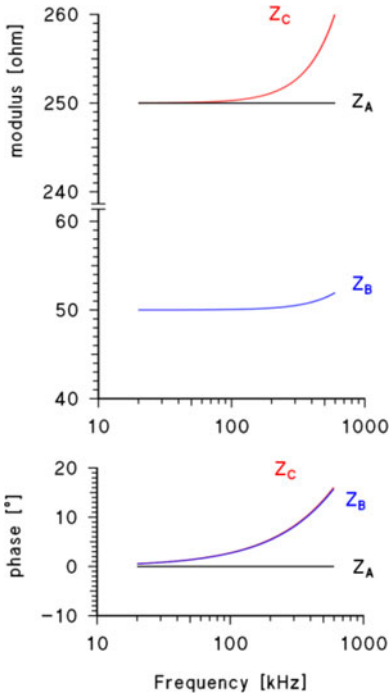

Fig. 13. Impedance magnitude and phase of the three segments of Fig.12; Z_C simulates the arm impedance, Z_B the trunk impedance and Z_A the leg impedance.

flow through C_{I2} and C_{SC}, these capacitances do not influence V_A, V_B, and V_C because they are directly driven by the amplifier output. Z_A, Z_B, and Z_C were calculated with a circuital simulator (OrCAD Capture CIS 16.6, 2011, Cadence Design Systems Inc, San Jose, CA, USA) between 20 and 600 kHz. Results (see Fig. 13) confirm that the measured impedance of body segment A is not affected by stray capacitances while measures of segments B and C show inductive effects.

REFERENCES

[1] A. Stahn, E. Terblanche, and H. C. Gunga, "Use of bioelectrical impedance: General principles and overview," in *Handbook of Anthropometry: Physical Measures of Human Form in Health and Disease*, V. R. Preedy, Ed. New York, NY, USA: Springer, 2012, pp. 49–90.

[2] M. Y. Jaffrin and H. Morel, "Body fluid volumes measurements by impedance: A review of bioimpedance spectroscopy (BIS) and bioimpedance analysis (BIA) methods," *Med. Eng. Phys.*, vol. 30, no. 10, pp. 1257–1269, Dec. 2008.

[3] L. W. Organ, G. B. Bradham, D. T. Gore, and S. L. Lozier, "Segmental bioelectrical impedance analysis: Theory and application of a new technique," *J. Appl. Physiol.*, vol. 77, no. 1, pp. 98–112, Jul. 1994.

[4] G. Sverre and G. M. Ørjan, *Bioimpedance and Bioelectricity Basics*, 2nd ed. Oxford, U.K.: Elsevier Academic Press, 2008.

[5] S. B. Rutkove, "Electrical impedance myography: Background, current state, and future directions," *Muscle Nerve*, vol. 40, no. 6, pp. 936–946, Dec. 2009.

[6] E. Raaijmakers, T. J. Faes, J. M. Meijer, P. W. Kunst, J. Bakker, H. G. Goovaerts, and R. M. Heethaar, "Estimation of non-cardiogenic pulmonary oedema using dual-frequency electrical impedance," *Med. Biol. Eng. Comput.*, vol. 36, no. 4, pp. 461–466, Jul. 1998.

[7] L. C. Ward, "Bioelectrical impedance analysis: Proven utility in lymphedema risk assessment and therapeutic monitoring," *Lymphat. Res. Biol.*, vol. 4, no. 1, pp. 51–56, 2006.

[8] F. Villa, A. Magnani, and P. Castiglioni, "Portable body impedance system for long-term monitoring of body hydration," in *Proc. 8th Conf. Ph.D. Res. Microelectron. Electron.*, 2012, pp. 229–232.

[9] H. P. Schwan and C. F. Kay, "The conductivity of living tissues," *Ann. N. Y. Acad. Sci.*, vol. 65, no. 6, pp. 1007–1013, Aug. 1957.

[10] L. A. Geddes and L. E. Baker, "The specific resistance of biological material–A compendium of data for the biomedical engineer and physiologist," *Med. Biol. Eng.*, vol. 5, no. 3, pp. 271–293, May 1967.

[11] F. Zhu, D. Schneditz, E. Wang, and N. W. Levin, "Dynamics of segmental extracellular volumes during changes in body position by bioimpedance analysis," *J. Appl. Physiol.*, vol. 85, no. 2, pp. 497–504, Aug. 1998.

[12] M. P. Bolton, L. C. Ward, A. Khan, I. Campbell, P. Nightingale, O. Dewit, and M. Elia, "Sources of error in bioimpedance spectroscopy," *Physiol. Meas.*, vol. 19, no. 2, pp. 235–245, May 1998.

[13] W. D. van Marken Lichtenbelt, K. R. Westerterp, L. Wouters, and S. C. Luijendijk, "Validation of bioelectrical-impedance measurements as a method to estimate body-water compartments," *Amer. J. Clin. Nutr.*, vol. 60, no. 2, pp. 159–166, Aug. 1994.

[14] A. De Lorenzo, A. Andreoli, J. Matthie, and P. Withers, "Predicting body cell mass with bioimpedance by using theoretical methods: A technological review," *J. Appl. Physiol.*, vol. 82, no. 5, pp. 1542–1558, May 1997.

[15] S. Grimnes and O. G. Martinsen, "Sources of error in tetrapolar impedance measurements on biomaterials and other ionic conductors" 40 ed. 2007, pp. 9–14.

[16] H. Scharfetter, P. Hartinger, H. Hinghofer-Szalkay, and H. Hutten, "A model of artefacts produced by stray capacitance during whole body or segmental bioimpedance spectroscopy," *Physiol. Meas.*, vol. 19, no. 2, pp. 247–261, May 1998.

[17] C. Aliau-Bonet and R. Pallas-Areny, "On the effect of body capacitance to ground in tetrapolar bioimpedance measurements," *IEEE Trans. Biomed. Eng.*, vol. 59, no. 12, pp. 3405–3411, Dec. 2012.

[18] A. Salceanu, O. Neacsu, V. David, and E. Lunca, "Measurements upon human body capacitance: Theory and experimental setup," in *Proc. 15th Symp. Novelties Elect. Measurements Instrum. Parallel With 12th Workshop ADC Modelling Testing*, Iasi, Romania, 2007.